Spectral Properties of Ca-sulfates: Gypsum, Bassanite and Anhydrite

Janice L. Bishop[1], Melissa D. Lane[2], M. Darby Dyar[3], Sara J. King[1],
Adrian J. Brown[1], and Gregg Swayze[4]

[1]SETI Institute, Carl Sagan Center, Mountain View, CA, 94043, USA.
[2]Planetary Science Institute, 1700 E. Fort Lowell Rd., Suite 106, Tucson, Arizona, USA.
[3]Mount Holyoke College, Department of Astronomy, South Hadley, MA, 01075, USA.
[4]U.S. Geological Survey, Denver, CO 80225, USA.

Keywords:
gypsum, sulfate, reflectance spectra, emission spectra, infrared

Revision 1

Submitted to American Mineralogist, September 25, 2013
Revised April 30, 2014

Abstract

This study of the spectral properties of Ca-sulfates was initiated in order to support remote detection of these minerals on Mars. Gypsum, bassanite and anhydrite are the currently known forms of Ca-sulfates. They are typically found in sedimentary evaporites on Earth, but can also form via reaction of acidic fluids associated with volcanic activity. Reflectance, emission, transmittance and Raman spectra are discussed here for a variety of sample forms. Gypsum and bassanite spectra exhibit characteristic and distinct triplet bands near 1.4-1.5 μm, a strong band near 1.93-1.94 μm, and multiple features near 2.1-2.3 μm attributed to H_2O. Anhydrite, bassanite and gypsum all have SO_4 combination and overtone features from 4.2-5 μm that are present in reflectance spectra. The mid-IR region spectra exhibit strong SO_4 ν_3 and ν_4 vibrational bands near 1150-1200 and 600-680 cm^{-1} (~8.5 and 16 μm), respectively. Additional weaker features are observed near 1005-1015 cm^{-1} (~10 μm) for ν_1 and near 470-510 cm^{-1} (~20 μm) for ν_2. The mid-IR H_2O bending vibration occurs near 1623-1630 cm^{-1} (~6.2 μm). The visible/near-infrared region spectra are brighter for the finer-grained samples. In reflectance and emission spectra of the mid-IR region the ν_4 bands begin to invert for the finer-grained samples, and the ν_1 vibration occurs as a band instead of a peak and has the strongest intensity for the finer grained samples. The ν_2 vibration is a sharp band for anhydrite and a broad peak for gypsum. The band center of the ν_1 vibration follows a trend of decreasing frequency (increasing wavelength) with increasing hydration of the sample in the transmittance, Raman and reflectance spectra. Anhydrite forms at elevated temperatures compared to gypsum, and at lower temperature, salt concentration, and pH than bassanite. The relative humidity controls whether bassanite or gypsum is stable. Thus, distinguishing among gypsum,

43 bassanite and anhydrite via remote sensing can provide constraints on the geochemical
44 environment.
45
46

Introduction

Common forms of Ca-sulfate are anhydrite $CaSO_4$, bassanite $CaSO_4 \bullet 0.5H_2O$ and gypsum $CaSO_4 \bullet 2H_2O$ (e.g. Dyar et al. 2008). Anhydrite typically forms at higher temperatures and gypsum at lower temperatures (Hardie 1967; Deer et al. 1992) and transformations between these two forms of Ca-sulfates do not occur readily under dry conditions at low temperatures. Gypsum, bassanite and anhydrite are all common sedimentary minerals found in marine evaporite sequences on Earth (Prothero and Schwab 2004). They can also occur as hydrothermal veins (Deer et al. 1992). Ca-sulfates have important industrial applications and are components of drywall, plaster and cement (e.g. Singh and Garg 1995; Dyar et al. 2008).

Gypsum is one of the first minerals precipitated from seawater of normal salinity because Ca^{2+} and SO_4^{2-} are less soluble than other ions. Thick, extensive gypsum deposits are less common than smaller outcrops, but are observed in shallow basin environments (Hardie and Eugster 1971). Gypsum generally forms at temperatures below 60°C (Conley and Bundy 1958) , while anhydrite forms at elevated temperatures and increased Ca^{2+} and SO_4^{2-} brine concentration (Billo 1987). Gypsum can also form from sulfuric acid solution or vapors through fumarole activity and it is also found in ash and ejecta blocks (Belousov 1995; Holland 2002). Bassanite is characteristic of dry marine evaporitic environments (Gunatilaka et al. 1985) and dry lake beds (Allen and Kramer, 1953).

Gypsum and bassanite have been detected in several regions on Mars in data from the Compact Reconnaissance Imaging Spectrometer for Mars (CRISM) data (e.g. Murchie et al. 2009) and the Observatoire pour la Minéralogie, l'Eau, lesGlaces et l'Activité (OMEGA) data (e.g. Bibring et al. 2005) using the characteristic near-infrared (NIR) spectral features near

1.5, 1.9 and 2.2 μm. Because pure anhydrite spectra do not contain features in this range it is more difficult to detect anhydrite in CRISM and OMEGA images. The SO_4 overtones and combinations observed from 4.2-5 μm are included in the spectral range covered by OMEGA; however, features in this range for Ca-sulfates have not yet been observed on Mars. This spectral region poses additional challenges because both reflectance and thermal emission contribute to the spectra here (Blaney and Mccord 1995). The Thermal Emission Spectrometer (TES) data covers the spectral range ~5.8-50 μm or 200-1724 cm^{-1} where the fundamental SO_4 vibrations are observed. Sulfates are often present at minor abundances in the TES model results, but at levels below what is needed to confidently identify them in the surface material (Christiansen et al. 2001), possibly because the sulfate features occur in the same spectral range as the atmospheric and surface dust that are confounding sulfate identification. The dust may also contain some sulfate. If the sulfates are fine-grained that would result in shallow diagnostic features as well, which would be difficult to discern.

Gypsum is the most common form of Ca-sulfate found on Mars. It has been identified at Olympia Undae (Langevin et al. 2005; Fishbaugh et al. 2007; Szumila et al. 2013), Meridiani Planum (Grotzinger et al. 2005; Squyres 2012), and Noctis Labyrinthus (Weitz et al. 2013a). Bassanite has been found at Mawrth Vallis (Wray et al. 2010).

The spectral properties of anhydrite, bassanite and gypsum are useful for remote detection of these minerals on the Earth and Mars. Many past studies have presented data of these minerals individually for a limited wavelength region (Miller and Wilkins 1952, Miller et al. 1960, Moenke 1962, Hunt et al. 1971, Ross 1974, McMillan and Hofmeister 1988, Crowley 1991, Bishop et al. 2004, Lane 2007, Harrison 2012) or published the

spectra as part of a library without interpretation of the spectral features (Salisbury et al. 1991, Clark et al. 2007). The objective of this study is to present a coordinated analysis of the spectral features of all three Ca-sulfate minerals with respect to their structures across the visible and infrared regions where remotely sensed spectra are used for detection of these minerals. Through coordinated analysis of the mid-infrared fundamental vibrations and the near-infrared overtones and combinations, band assignments can be made and confirmed.

Background

Gypsum is the most common sulfate mineral and has been known since the time of the Greeks (e.g. Bromehead 1943). Gypsum occurs as clear crystals called selenite or as massive material called alabaster. Anhydrite was named after the Greek word for "without water" (Ludwig 1804) and can be vitreous, greasy and pearly. Both gypsum and anhydrite are prevalent in evaporite deposits of marine origin in numerous sites on Earth (e.g. Billo, 1987). Anhydrite is harder and more dense than gypsum (e.g. Deer et al. 1992); δ_{gypsum} is ≈2.3 g/cm^3, while $\delta_{anhydrite}$ is ≈2.9 g/cm^3 (Robertson et al. 1958). Gypsum is the main constituent of the dunes at the White Sands National Monument in New Mexico (e.g. Szynkiewicz et al. 2010) and is present at 95-99 wt.% in much of the dune sand (Fenton et al. 2014; Lafuente et al. 2014).

Particulate anhydrite will slowly react to form gypsum at low temperatures when water is added, making it a useful component of cement (e.g. Sievert et al. 2005). Gypsum and anhydrite are often located together when large marine evaporite deposits were formed under variable temperatures (Appleyard 1983; Haynes et al. 1989). Halite is also

116 frequently found with anhydrite and gypsum when the evaporitic brine contains Na^+, Ca^{2+},
117 Cl^- and SO_4^{2-} (e.g. Posnjak 1940; Robertson et al. 1958; Leitner et al. 2013)
118 Bassanite was originally found in volcanic settings as leucite tephra blocks at Vesuvius,
119 Italy, and was named after Francesco Bassani (Zambonini 1910). Bassanite is also known
120 as plaster of Paris and as hemihydrate (e.g. Singh and Middendorf 2007). It has been found
121 in dry lake beds in California (Allen and Kramer 1953), in rocks along the coast of England
122 (Worku and Parker 1992), Indiana (Bundy 1956), and the Arabian Gulf (Gunatilaka et al.
123 1985). Bassanite is a metastable mineral that forms when gypsum and anhydrite are in
124 transition (Bundy 1975) and frequently occurs following dissolution and reprecipitation of
125 gypsum (Worku and Parker 1992). Bassanite is present in marine evaporitic environments
126 in the dry summer season in Kuwait and hydrates to gypsum in the wet winter months
127 (Gunatilaka et al. 1985).
128
129 **Mineral Structures of Ca-Sulfates**
130 Gypsum, bassanite and anhydrite are all monoclinic (e.g. Dyar et al. 2008). The
131 structures are based on large coordination polyhedra needed to accommodate the Ca^{2+}
132 cation, so Ca is generally 8- or 9-coordinated. Most forms of Ca-sulfates are variations on
133 the anhydrite structure, which consists of alternating chains of Ca dodecahedra sharing
134 edges with SO_4 tetrahedra (e.g. Dyar et al. 2008). As seen in Figure 1, bassanite and gypsum
135 represent slight variations on the anhydrite structure. In bassanite, the Ca cation is 9-
136 coordinated, and the chains of alternating edge-sharing trigonal prisms and sulfate
137 tetrahedra connect to form a framework. The gypsum structure is quite similar to that of
138 anhydrite, although the repeat distance between the chains is slightly longer for gypsum

and O^{2-} is replaced by H_2O at two of the unshared corners of each 8-coordinated Ca site. The compactness of these structures depends on how many H_2O groups are in each mineral, and on the number of alkali elements (Hawthorne et al. 2000). Anhydrite and bassanite have no or 0.5 H_2O per unit formula, respectively, and the chains are linked into three-dimensional frameworks. Gypsum has 2 H_2O molecules per formula unit, resulting in a sheet structure with H- bonding between water molecules in adjacent chains.

Bassanite generally exists as monoclinic α-hemihydrate but can also exist as triclinic β-hemihydrate when formed in specific synthetic environments (Singh and Middendorf 2007). The α-hemihydrate is formed from gypsum at temperatures above 45 °C in acidic environments or salt solutions or above 97 °C in water and is the most common form of bassanite. The β-hemihydrate is made by calcining gypsum under low water vapor pressure or under vacuum at 45-200 °C (Singh and Middendorf 2007).

Spectral Properties of Ca-Sulfates

Early visible/near-infrared (VNIR) reflectance spectra of sulfates were presented by Hunt and Salisbury (1971) and illustrated that the dominant VNIR bands are due to H_2O near 1.4-1.5 and 1.9-2.0 μm. More recent NIR sulfate spectra demonstrated that both OH and H_2O are responsible for most features in the 1-3 μm range (Clark et al. 1990; Crowley 1991; Bishop and Murad 1996; Bishop and Murad 2005; Cloutis et al. 2006); however, features near 4.3-5.3 μm are attributed to overtones and combinations of the v_3 SO_4 asymmetric stretching vibration (Blaney and Mccord 1995; Bishop and Murad 2005). Hunt and Salisbury (1971) identified bands near 1.0, 1.2, 1.4-1.5, 1.75 and 1.9-2.0 μm in spectra of gypsum. Crowley (1991) showed that bassanite spectra have similar features to gypsum

spectra, but that many bands are sufficiently distinct for differentiation of these minerals. Experiments by Harrison (2012) showed that the characteristic gypsum bands shift towards shorter wavelengths as the sample is converted to bassanite. However, the specific wavelengths of each of these features in gypsum and bassanite spectra have not been presented and analyzed in past studies. Anhydrite should be anhydrous and thus featureless near 1.4 and 1.9 μm, but spectra of many "anhydrite" specimens do show weak features here indicating that they are partially hydrated and possibly in transition to bassanite or gypsum (Cloutis et al. 2006).

Mid-infrared (mid-IR) transmission spectra of sulfates were summarized by Ross (1974) and include features near 980 cm^{-1} for the SO_4 ν_1 symmetric stretching vibration, near 450 cm^{-1} for the SO_4 ν_2 symmetric bending vibration, near 1100 cm^{-1} for ν_3 and near 610 cm^{-1} for the SO_4 ν_4 asymmetric bending vibration. Early studies of gypsum spectra describe strong bands at 603, 668, 1130, 1630, 2200, and 3410 cm^{-1}, plus weak bands at 1010 and 1670 cm^{-1} (Miller and Wilkins 1952; Miller et al. 1960). The frequencies of the ν_1, ν_2, ν_3, and ν_4 sulfate modes are generally similar for all Ca-sulfates in transmission (Moenke 1962), Raman (Prasad et al. 2001) and emission (Lane 2007) data. Small shifts toward higher frequencies were observed for ν_1 and ν_2 from gypsum to bassanite to anhydrite in transmission spectra (Moenke 1962; Ross 1974). Triplets were observed near 1100-1150 cm^{-1} for ν_3 and near 590-675 cm^{-1} for ν_4 in all Ca-sulfate spectra (Moenke 1962; Ross 1974), and this relative shift to higher frequencies with less water in the structure was seen in emission data for the ν_3 and lattice modes (Lane 2007). Additional H_2O stretching (νH_2O) features are observed for bassanite near 3465 and 3615 cm^{-1} and for gypsum at 3250, 3408, 3500 and 3555 cm^{-1}, and H_2O bending (δH_2O) vibrations occur at 1629 cm^{-1} for

bassanite and at 1629 and 1690 cm^{-1} for gypsum (Ross, 1974) in the transmission data. Mid-IR emission data show the δH_2O band at ~1630 cm^{-1} for bassanite and at 1621 cm^{-1} for gypsum (Lane, 2007).

Raman spectra of gypsum, bassanite, and anhydrite exhibit similar trends with a single absorption due to the ν_1 vibration present at 1004 – 1016 cm^{-1}, ν_2 as a doublet near 414-438 and 490-498 cm^{-1}, ν_3 as a triplet near 1110-1160 cm^{-1} and ν_4 as a triplet at ~602-670 cm^{-1} (Berenblut et al. 1973; Prasad et al. 2001; Prasad et al. 2005).

Formation and Stability of Ca-Sulfates

Early investigations of marine evaporites suggested that gypsum was always deposited first and then partially converted to anhydrite in some cases (e.g. Murray 1964). However, Billo (1987) noted that many ancient marine evaporite deposits contain anhydrite at depth with gypsum on the surface or alternating laminae of anhydrite and other minerals, suggesting that other formation paths exist for anhydrite. It can form as a primary evaporative mineral under conditions of elevated temperatures, increased Ca^{2+} and SO_4^{2-} brine concentration and/or the presence of organic matter (Billo 1987). Experiments by Meijer (1984) on Ca-sulfate solubility at variable temperature, pH and salt concentration of sea water showed that gypsum precipitation is favored at 1 atm where there are high salt concentrations and temperatures below 40 °C, while anhydrite generally forms at temperatures ~40-120 °C and pH ~6-7. Bassanite forms at higher temperatures (favored above 120 °C, but possible above 80 °C) than anhydrite and at a higher pH range of ~8-9. Generally anhydrite forms under lower salt concentrations and bassanite at higher salt

concentrations. However, anhydrite becomes less soluble than bassanite and will preferentially precipitate out at a pH of 6 even for higher salt concentrations.

Many researchers have studied the transformation of gypsum and anhydrite and found that gypsum is more prevalent at lower temperatures, while anhydrite is the stable form at higher temperatures (e.g. Ostroff 1964, Innorta 1980, Kushnir 1982; Zhang et al. 1996, Sievert et al. 2005). Early experiments showed that conversion occurs as gypsum changes to bassanite and then anhydrite (Conley and Bundy 1958; Ostroff 1964). Ostroff (1964) found that particulate gypsum reacted in salt solution at 90 °C to form anhydrite in a few days, while the reaction of gypsum in pure Ca-sulfate solution required temperatures above 97 °C. Gypsum and bassanite were converted to anhydrite in brine solution at 83 °C, where the gypsum needles were clearly observed to disappear as tiny anhedral anhydrite crystals were formed (Kushnir 1982). These experiments demonstrated that formation of bassanite was not a requirement in the phase transformation from gypsum to anhydrite, as confirmed by Prasad et al. (2005). Another study showed that bassanite will never form below ~88 °C (Ridge and Beretka, 1969). Billo (1987) observed that gypsum can be converted to bassanite in pure water at temperatures over 100 °C and then converted to anhydrite, but that bassanite cannot be derived from anhydrite at any temperature. Anhydrite can be dissolved in solution and then reprecipitated as gypsum under low temperature conditions. Sievert et al. (2005) studied gypsum formation from anhydrite in solution and found that this was faster at temperatures below 40 °C. However, the anhydrite must be at least partially dissolved first; gypsum cannot be formed directly by hydrating anhydrite (e.g. Prasad et al. 2005).

Innorta et al. (1980) investigated gypsum solubility in pure water and found an equilibrium temperature of 49.5 ± 2.5 °C, while Hardie (1967) found the equilibrium temperature for gypsum and anhydrite solubilities to be 58 °C. Billo (1987) states that kinetic considerations are also important in understanding gypsum-anhydrite equilibria in solution and that grain size and hardness contribute to the solubility of Ca-sulfates.

Conversion of anhydrite to gypsum has been studied in detail by the cement industry. Singh and Garg (1995) describe a dissolution-nucleation growth process where Ca is separated from SO_4 in anhydrite by activator salts and then gypsum is precipitated as the Ca and sulfate react again in solution. Experiments by Sievert et al. (2005) suggest that partially dissolved anhydrite grains serve as nucleation centers for adsorbed hydrated Ca-sulfate to form. As the adsorbed layer of hydrated Ca-sulfate gets thicker, cracks form in the adsorbed layer enabling migration of H_2O and complete conversion of the anhydrite to gypsum. These experiments showed that gypsum formed progressively faster as the temperature was dropped from 40 to 20 to 10 °C (Sievert et al. 2005). Dry grinding of gypsum was found to produce some bassanite after only 15 minutes, but the reaction only continued completely in the presence of clay additives; 35 wt.% talc was found to be the most effective agent tested (Zhang et al. 1996). Additives also influenced the morphology of gypsum crystals and the rate kinetics (Badens et al. 1999).

Methods

The samples in this study were obtained from multiple sources (e.g. collected in North America, Europe, Africa or synthesized in the lab) and are listed in Table 1. For sample JB1464 a gypsum rock was crushed and any dark grains were removed. The grains were

gently ground in a mortar and pestle and dry sieved into several grain sizes. The 45-90 μm fraction was wet sieved with methanol in addition to remove fines. The ML-S6 gypsum sample was wet sieved at the time of preparation in 1993. The 63-90 μm (JB557) size fraction was rewashed in 2000 before reflectance spectra were measured. The <63 μm size fraction appears to have partially altered to bassanite by the time the reflectance spectra were run in 2000. Spectra were also measured for this study of gypsum samples JB1464a-e and the anhydrite sample JB641. The bassanite sample from the USGS collection (Clark et al. 2007) is GDS145, formed by heating gypsum at 60 °C by Crowley (1991). One anhydrite sample (JB641, DD102) contains minor admixtures that contribute an iron band, but no hydration features, while another anhydrite sample (GDS42 from the USGS collection) (Clark et al. 2007) is slightly hydrated and contains a weak iron band.

Measurement of reflectance spectra

Reflectance spectra were measured for this study at Brown University's RELAB using a bidirectional VNIR spectrometer under ambient conditions relative to Halon and a biconical Nicolet Fourier Transform Infrared (FTIR) spectrometer in a controlled, dry environment relative to a rough gold surface as in previous studies (e.g. Bishop and Murad 2005). The bidirectional spectra were acquired from 0.3 to 2.5 μm at 5 nm spectral sampling. Infrared reflectance spectra were measured with 2 cm^{-1} spectral sampling from 1-50 μm in an environment purged of H_2O- and CO_2- for 10-12 hours. Composite, absolute reflectance spectra were prepared by scaling the FTIR data to the bidirectional data near 1.2 μm.

Additional FTIR reflectance spectra were collected at the USGS Spectroscopy

Laboratory (Clark et al. 2007), available online at http://speclab.cr.usgs.gov/ and from Salisbury et al. (1991). The Salisbury spectral archive includes hemispherical reflectance spectra of grains <75, 75-250 μm, and mineral surfaces.

A continuum was removed from the spectra across the ranges 1.28-1.64, 2.05-2.35 and 3.8-5.0 μm of selected spectra in order to facilitate comparison of the band strengths proposed in Brown (2006) and implemented in Brown et al. (2008).

Measurement of emission spectra

The emitted radiation from various mineral and rock samples was measured by Lane (2007) using a modified Nicolet Nexus 670 FTIR interferometric spectrometer over the range of 2000 to 200 cm^{-1} with 2 cm^{-1} spectral sampling. The gypsum samples were measured at ~50 °C and the others at ~ 80 °C. Two blackbody targets (at ~70 and 100 °C) were measured to determine the instrument response function and instrument temperature used for data calibration. The emission spectra of the minerals were obtained by reducing the raw wavelength and temperature-dependent data according to the one-temperature procedure of Ruff et al. (1997), assuming that sample emission equals unity at the Christiansen feature (e.g. Logan et al. 1975; Salisbury 1993).

Measurement of transmittance spectra

Transmittance spectra were measured by Salisbury et al. (1991) of one anhydrite and two gypsum samples by mixing the minerals with KBr to prepare pellets for analysis.

Results

VNIR spectra

Hydrated Ca-sulfates exhibit a characteristic triplet near 1.4 μm and strong features near 1.9, 2.8-3.1 and 4.2-5 μm (Figure 2). The triplet occurs at 1.446, 1.490, and 1.538 μm for gypsum and at 1.428, 1.476, and 1.540 μm for bassanite (Figure 3, Table 2). Another triplet is observed in spectra of gypsum at 2.178, 2.217, and 2.268 μm; however, spectra of bassanite exhibit multiple weaker features here at 2.10, 2.164, 2.219, 2.262 and 2.268 μm (Figure 4, Table 2). An additional band is observed at 2.268 μm in gypsum spectra and as a doublet at 2.262 and 2.268 μm in bassanite spectra. These are attributed to H_2O as well because they are not observed for anhydrite. Interestingly, the partially hydrated anhydrite spectrum has a shoulder feature here (Figure 2).

Spectra of all Ca-sulfates exhibit multiple combination and overtone features near 4.2-5 μm (Figure 5). Anhydrite spectra provide several distinct bands, while the spectra of bassanite and gypsum include broader features of overlapping bands. The anhydrite features occur at 4.203, 4.286, 4.348, 4.469, 4.668, 4.691, and 4.925 μm (Table 2). Besides the overlap-broadened features in this region, the distinguishing feature of gypsum and bassanite spectra compared to anhydrite spectra is a shift of the band at 4.925 to ~4.97 μm for bassanite and gypsum.

Mid-IR spectra

The strongest mid-IR bands are due to SO_4 ν_3 and ν_4 vibrations (Figures 6-7). Additional deep bands are seen in the ,emission data that result from metal-oxygen or lattice modes

(Lane, 2007). The ν_3 vibration is observed as a doublet or triplet near 1150-1200 cm^{-1} (Table 2) and the ν_4 vibration is observed as a doublet or triplet near 600-690 cm^{-1}. The nature of these bands is dependent on grain size with finer grained samples exhibiting shoulders and additional spectral character in the region between the fundamental bands, as well as a weakening of the fundamental bands (Lane and Christensen 1998). Transmittance spectra exhibit sharp triplets for both ν_3 and ν_4 (Figure 8, Ross 1974, Salisbury et al. 1991). These triplets are also seen in the transmission spectra of bassanite and anhydrite of Moenke (1962). However, in the gypsum spectrum of Moenke (1962), ν_3 and ν_4 are represented by doublets, but these doublets have spectral character (i.e., a band broadening) that indicates a third band for both the ν_3 and ν_4, but these third bands are largely degenerate.

The ν_1 vibration is observed as an absorption band at 1015, 1012 and 1005 cm^{-1}, respectively, for anhydrite, bassanite and gypsum in reflectance spectra (Figures 6-7) and is stronger for fine-grained samples. Transmittance spectra of anhydrite and gypsum also have a weak to very weak ν_1 feature (Figure 8, Ross 1974, Moenke 1962). The bassanite transmission spectrum of Moenke (1962) shows the ν_1 feature to be much stronger and more apparent.

The ν_2 vibration is seen at 510 cm^{-1} in reflectance/emission spectra of fine-grained anhydrite, but is difficult to detect in spectra of coarse-grained samples or surfaces (Figures 6-9). Transmittance spectra of anhydrite show this feature at 515 cm^{-1} (Figure 8, Ross 1974; Moenke 1962). The broader, weaker ν_2 bands occur at lower frequencies in reflectance and emission spectra (Figures 6-7) and as doublets at lower frequencies for bassanite and gypsum in transmittance spectra (Ross, 1974).

Additional weak bands are observed at 843, 894, 1543 cm^{-1} for reflectance spectra of fine-grained anhydrite (Figures 6 and 9), but are not found in transmittance spectra or in reflectance/emission spectra of the coarse-grained samples or the mineral surfaces.

Effects of Grain Size and Relative Humidity

The effects of grain size are shown in the mid-IR region for gypsum in Figure 10, where the ν_3 and ν_4 modes increase in intensity with increasing grain size. The ν_2 mode remains about the same for most spectra, but is not observed in the spectrum of the finest size fraction, while the ν_1 mode becomes more obvious with decreasing grain size (Figure 10, Lane and Christensen 2008). Additional δH_2O bands near 1600-1700 cm^{-1} increase in intensity, and lattice modes near 150-250 cm^{-1} decrease in intensity with decreasing grain size. The emission and biconical reflectance spectra of the >250 μm gypsum are similar; however, the shape of the ν_3 triplet near 1150-1200 cm^{-1} differs.

The effects of grain size on the VNIR spectra of gypsum are shown in Figure 11. The spectral brightness and band depth for all features increases with decreasing grain size. The VNIR bands are dependent on relative humidity as well as grain size. Spectra of three size fractions are shown in Figure 12 that were measured under ambient and dehydrated conditions (air purged of H_2O and CO_2). A systematic trend can be seen for increasing band depth for the H_2O features in the spectra measured under ambient conditions compared to those measured under H_2O-purged conditions.

Discussion

ν_3 vibrations

The dominant ν_3 vibrations for anhydrite occur at 1121 and 1159 cm^{-1} in the transmittance spectra of Salisbury et al. (1991, Figure 9), at 1095, 1126, and 1149 cm^{-1} in the Ross (1974) data and at 1130 and 1159 cm^{-1} in the Moenke (1962) data. They occur instead at 1155, 1167 and 1201 cm^{-1} in reflectance data of an anhydrite surface (Figure 9, Salisbury et al. 1991) and at 1158 and 1200 cm^{-1} in emission data of an anhydrite surface (Figure 7, Lane 2007). A shoulder near 1240 cm^{-1} in the reflectance spectrum of the anhydrite surface becomes stronger for the spectrum of the 75-250 μm size fraction of anhydrite. For the <75 μm anhydrite reflectance spectrum the ν_3 vibration is a doublet with the strongest peak at 1236 and another peak at 1213 cm^{-1} and a shoulder at 1154 cm^{-1}. The ν_3 Raman triplet bands occur at 1124 and 1157 cm^{-1} for anhydrite (Prasad et al. 2005).

The ν_3 vibrations in bassanite spectra exhibit more character than in the spectra of gypsum or anhydrite. They are observed at 1100, 1120, and 1158 cm^{-1} with a shoulder near 1180 cm^{-1} in transmittance spectra (Moenke 1962) and at 1096, 1116, 1153 and 1168 cm^{-1} in Raman spectra (Prasad et al., 2005), while they occur at 1090, 1117, 1157 and 1172 cm^{-1} with a shoulder near 1200 cm^{-1} in reflectance data (Figure 6), and at 1092, 1122 and 1157 cm^{-1} with a shoulder near 1185 cm^{-1} in emission data (Figure 7, Lane 2007).

Gypsum exhibits a similar trend for the ν_3 vibrations (Figure 9, Salisbury et al. 1991) with transmittance bands at 1096, 1130, and 1155 cm^{-1} (Figure 9) in the Salisbury et al. (1991) data, as a triplet at 1117, 1138 and 1144 cm^{-1} or 1118, 1131 and 1142 cm^{-1} in the Ross (1974) data, and as a doublet at 1120 and 1150 cm^{-1} with a shoulder at higher

389 wavenumbers in the Moenke (1962) data. A triplet is observed at 1117, 1145 and 1167 cm-
390 ^{1} for the ν_3 vibrations in Raman spectra of gypsum (Prasad et al. 2005). Gypsum surface
391 spectra exhibit a band at 1165 cm^{-1} with a shoulder near 1200 cm^{-1} in reflectance data
392 (Figure 9, Salisbury et al. 1991) and a band at 1154 cm^{-1} with a shoulder near 1200 cm^{-1} in
393 emission data (Figure 7, Lane 2007). The ν_3 vibration becomes a peak at 1200 cm^{-1} in
394 reflectance spectra of the fine-grained samples (Figures 9b and 10).

395 Differences are observed between transmittance spectra peak positions and
396 reflectance/emission spectra peak positions because transmittance spectra depend only on
397 the absorption properties, while reflectance and emission spectra are a function of both the
398 real, *n*, and imaginary, *k*, indices of refraction (e.g. Logan et al. 1975; Hapke 1981; Mcmillan
399 and Hofmeister 1988). Reflectance and emission spectra in the mid-IR region are
400 dominated by surface scattering for coarse grained materials or surfaces resulting in strong
401 reststrahlen bands and by volume scattering for fine particles resulting in weaker
402 reststrahlen bands and strong transparency features (Salisbury and Wald 1992; Mustard
403 and Hays 1997; Lane 1999; Bishop et al. 2004). For this reason reflectance and emission
404 spectra also vary with grain size. For materials like Ca-sulfates where the refractive index is
405 ~1.5 some of the mid-IR vibrational features invert from bands to peaks (i.e. the ν_3 mode at
406 1110 cm^{-1} in Figures 9-10). Other minerals have higher indices of refraction and do not
407 exhibit this trend (Dyar et al. 2008). The inversion from bands to peaks with grain size is
408 also observed for mid-IR spectra of calcite (Salisbury and Wald 1992; Lane and Christensen
409 1998; Lane 1999), which has a refractive index ~1.5 (Dyar et al. 2008). Reflectance (R) and
410 emission (E) spectra are related by Kirchhoff's Law, E=1-R, which generally holds for
411 hemispherical or off-axis reflectance spectra, but does not always work for smaller grains

(Hunt and Vincent 1968; Salisbury and Wald 1992; Hapke 1993; Wenrich and Christensen 1996).

ν_1 vibrations

The ν_1 vibration occurs as a single band in spectra of Ca-sulfates and follows a similar trend for transmittance, Raman, reflectance and emission spectra, where the vibrational energy shifts towards lower frequencies as the mineral becomes hydrated. The ν_1 band is observed at 1013, 1012 and 1006 cm^{-1} in transmittance spectra of anhydrite, bassanite and gypsum, respectively (Moenke 1962, Ross 1974), and is observed at 1014, 1008 and 1005 cm^{-1} in Raman spectra of anhydrite, bassanite and gypsum, respectively (Prasad et al. 2005). This feature is observed at 1015, 1012 and 1005 cm^{-1}, respectively, in reflectance spectra for fine-grained samples (Figure 6).

ν_4 vibrations

The ν_4 vibrations for anhydrite occur as a triplet at 596, 615, and 677 cm^{-1} in the transmittance spectra of Salisbury et al. (1991, Figure 9), at 592, 612, and 671 cm^{-1} in the Ross (1974) data and at 597, 616 and 676 cm^{-1} in the Moenke (1962) data. Raman vibrations for the anhydrite ν_4 mode are observed at 595, 615, and 676 cm^{-1} (Prasad et al., 2001). Restrahlen peaks are observed at 597, 619 and 687 cm^{-1} in reflectance spectra of an anhydrite surface (Figure 9, Salisbury et al. 1991) and bands are found at 596, 619, and 687 cm^{-1} in emission data (Figure 7, Lane 2007). As the grain size decreases, the ν_4 vibrations

433 invert and become absorptions instead of peaks. These are observed at 592, 613, and 669
434 cm^{-1} (i.e. spectra b vs d in Figure 9).

435 Transmittance spectra of bassanite have a triplet for the ν_4 mode that is observed at
436 605, 634 and 667 cm^{-1} (Moenke 1962; Ross 1974) and Raman spectra of bassanite have a
437 doublet at 601 and 660 cm^{-1} (Prasad et al. 2005). The bassanite ν_4 bands occur at 596 and
438 660 cm^{-1} in reflectance spectra (Figure 6) and at 598 and 663 cm^{-1} in emission spectra
439 (Figure 7, Lane 2007).

440 Gypsum spectra exhibit a doublet for the ν_4 mode that is observed in the transmittance
441 data of Salisbury et al. (1991, Figure 9) at 598 and 666 cm^{-1}, in the Ross (1974) data near
442 603 and 674 cm^{-1} or 622 and 669 cm^{-1}, and in the Moenke (1962) data at 605 and 673 cm^{-1}.
443 The ν_4 vibrations occur at 602 and 669 cm^{-1} in Raman spectra of gypsum (Prasad et al.
444 2005). Gypsum surface spectra exhibit a doublet at 604 and 678 cm^{-1} in reflectance data
445 (Figure 9, Salisbury et al. 1991) and bands at 604 and 677 cm^{-1} in emission data (Figure 7,
446 Lane 2007). Gypsum's ν_4 vibrations start to flip in reflectance spectra of the fine-grained
447 samples and exhibit multiple weak up and down features or peak reversals from 586-700
448 cm^{-1} (Figures 9-10).
449

450 **ν_2 vibrations**

451 The ν_2 vibration occurs as a very weak single band at 515 cm^{-1} in transmittance spectra
452 of anhydrite (Figure 9, Moenke 1962; Ross 1974; Salisbury et al 1991), while two bands at
453 424 and 490 cm^{-1} are observed for the ν_2 vibration in Raman spectra of anhydrite (Prasad

et al., 2001), and a single band is observed in fine-grained spectra of anhydrite, but not in surface spectra of anhydrite (Figure 9a).

Two broad, weak bands are observed near 420 and 465 cm^{-1} in transmittance spectra for the ν_2 vibration of bassanite (Moenke 1962), while two bands at 421 and 490 cm^{-1} are observed for the ν_2 vibration in Raman spectra of gypsum (Prasad et al., 2001). No bands were observed for the ν_2 vibration in reflectance and emission spectra of bassanite in our study.

A broad, weak band from about 415-490 cm^{-1} is observed in transmittance spectra for the ν_2 vibration of gypsum (Figure 9, Moenke 1962; Ross 1974; Salisbury et al 1991), while two bands at 420 and 494 cm^{-1} are observed for the ν_2 vibration in Raman spectra of gypsum (Prasad et al., 2001), and a weak, broad band is observed near 480 cm^{-1} in reflectance spectra and near 460 cm^{-1} in emission spectra of gypsum (Figure 7).

Characteristic features of Ca-sulfates

Gypsum and bassanite exhibit characteristic bands near 1.4-1.5, 1.93-1.94, and 2.1-2.3 μm due to H_2O vibrations and additional mostly broad bands from 4.2-5 μm due to SO_4 vibrations. Anhydrite spectra contain multiple individual bands from 4.2-5 μm due to SO_4 vibrations. The mid-IR region spectra exhibit strong SO_4 ν_3 vibrational bands near 1150-1200 cm^{-1} and ν_4 vibrational bands near 600-680 cm^{-1}. Additional weaker features are observed near 1005-1015 cm^{-1} for the ν_1 mode and near 470-510 cm^{-1} for the ν_2 mode. The mid-IR H_2O bending vibration occurs near 1623-1630 cm^{-1}. The visible/near-infrared region spectra are brighter and have deeper bands for the finer-grained samples. In the mid-IR region the ν_4 absorptions transition to peaks in spectra of the finer-grained

477 samples, the ν_1 vibration occurs as an absorption instead of a peak and has the strongest
478 intensity in spectra of the finer grained samples. The ν_2 vibration is a sharp band for
479 anhydrite and a broad peak for gypsum. The band center of the ν_1 vibration follows a trend
480 of decreasing frequency (increasing wavelength) with increasing hydration of the sample
481 in the transmittance, Raman and reflectance spectra. The ν_2 vibration tends to follow this
482 trend as well.
483

484 **Implications for Mars**

485 The largest gypsum deposit on Mars is present at the north polar sand dunes of the
486 Olympia Undae region (Langevin et al. 2005; Fishbaugh et al. 2007). Fishbaugh et al. (2007)
487 hypothesized that the gypsum in the dunes formed by water emanating from nearby
488 channels, while Masse et al. (2011) proposed the gypsum grains formed by weathering of
489 dust particles. Szumila et al. (2013) found that gypsum has a higher abundance in primary
490 dunes at Olympia Undae rather than secondary dunes that formed subsequently, indicating
491 that gypsum was likely present when the dunes formed and may be altering under current
492 conditions. No evidence was observed for changes in the form of the Ca-sulfate due to
493 modification of the dunes (Szumila et al. 2013).

494 Gypsum is also thought to be present in small veins observed in rocks at Endeavor
495 Crater by the Opportunity rover (Squyres et al. 2012). These are interpreted to have
496 formed as water flowed through cracks in the rocks that later became exposed at the
497 surface as the rocks were eroded (Squyres et al. 2012). Gypsum has also been found in
498 some rocks and soils of the Columbia Hills in Gusev crater (Squyres et al., 2006; Yen et al.,
499 2008). If a NIR spectrometer is sent to Mars on a future rover then the characteristic

features near 1.4-1.5, 1.93-1.94 and 2.1-2.3 μm could be used to determine if gypsum or bassanite were present in rocks or veins like these observed at Endeavor Crater and the Columbia Hills. Discovering this would provide constraints on the temperature and pH of the formation environment as gypsum generally forms below 40 °C at neutral pH and bassanite typically forms at temperatures above 120 °C and at pH 8-9.

Wray et al. (2011) used CRISM spectra to identify gypsum associated with Fe/Mg-sulfates in a discreet ring around the walls of Columbus crater, while Weitz et al. (2013b) found Ca-sulfate in outcrops along the western Melas Chasma floor and Weitz et al. (2013a) identified gypsum outcrops in a trough at Noctis Labyrithus. Mangold et al. (2010) observed Ca-sulfate in a separate Noctis Labyrithus trough farther to the east and suggested that local frost/snow reacted with Ca and S to form gypsum due to lack of evidence for evaporative processes. Weitz et al. (2013a) suggest that if hydrothermal conditions existed that enabled snow and ice to melt, then the associated heat would also allow gypsum to precipitate. As gypsum formation is favored over other Ca-sulfates at temperatures below ~40 °C, temperatures were likely not elevated much above this if hydrothermal processes took place.

Wray et al. (2010) observed bassanite in the floor of the outflow channel at Mawrth Vallis. The bassanite was found in topographic lows surrounded by exposures of Fe/Mg-smectites and the bassanite appears to have been emplaced prior to the clay-rich unit. This is contrary to the more commonly observed sequence of phyllosilicates in Noachian terrains and sulfates in younger Hesperian terrains (Bibring et al. 2006). Baldridge et al. (2009) reported fieldwork on sulfates from dry lakes in the Western Australian playa regions and suggested that sulfate deposition could take place contemporaneously with

phyllosilicate deposition within natural terrestrial settings. This work was guided by maps of sulfate in the dry lakes created from ASTER satellite data (Brown and Cudahy 2006). Spectra of bright units at Mawrth Vallis (e.g. Wray et al. 2010, Bishop et al. 2013) are not consistent with the presence of gypsum, although it is unknown if anhydrite is present. This indicates that the relative humidity is sufficiently low for the Ca-sulfate to remain in the bassanite state. Possibly the Ca-sulfate observed at Mawrth Vallis is fine-grained and more readily dehydrated to bassanite than in other locations such as the gypsum-bearing sand dunes at Olympia Undae. The clays at Mawrth Vallis may have also facilitated bassanite formation from gypsum through wind abrasion, as clays are an industrial additive for gypsum conversion to bassanite through grinding.

Spectral data presented here will enable more detailed identification of Ca-sulfates on Mars and may allow for grain size determinations in some outcrops. The variable temperature, pH and salt concentration regimes that govern which Ca-sulfate mineral forms can thus be used to provide constraints on the geochemical environment of Ca-sulfate outcrops on Mars using orbital and rover spectroscopy.

Acknowledgements

We are grateful for support from NASA's Mars Fundamental Research Program grant NNX11AF116. We also thank T. Hiroi at Brown University's RELAB for measuring many of the reflectance spectra used in the study and the PGGURP program for providing support for S. King. Thoughtful comments from Karly Pitman and an anonymous reviewer greatly improved the manuscript. Any use of trade, firm, or product names is for descriptive

purposes only and does not imply endorsement by the U.S. Government. This work is PSI Contribution Number 607.

References

Allen, R.D. and Kramer H. (1953) Occurrence of bassanite in two desert basins in southeastern California. American Mineralogist, 38, 1266–1268.

Appleyard, F.C. (1983) Gypsum and anhydriteEds., Industrial Minerals and Rocks (Nonmetallics Other than Fuels), 775-792. American Institute of Mining, Metallurgical, and Petroleum Engineers. New York, NY.

Badens, E., Veesler S., and Boistelle R. (1999) Crystallization of gypsum from hemihydrate in presence of additives. Journal of Crystal Growth, 198–199, 704-709.

Baldridge, A.M., Hook S.J., Crowley J.K., Marion G.M., Kargel J.S., Michalski J.L., Thomson B.J., de Souza Filho C.R., Bridges N.T., and Brown A.J. (2009) Contemporaneous deposition of phyllosilicates and sulfates: Using Australian acidic saline lake deposits to describe geochemical variability on Mars. Geophysical Research Letters, 36, 1-6.

Belousov, A.B. (1995) The Shiveluch volcanic eruption of 12 November 1964—explosive eruption provoked by failure of the edifice. Journal of Volcanology and Geothermal Research, 66, 357-365.

Berenblut, B.J., Dawson P., and Wilkinson G.R. (1973) A comparison of the Raman spectra of anhydrite (CaSO4) and gypsum (CaSO4).2H2O). Spectrochimica Acta Part A: Molecular Spectroscopy, 29, 29-36.

Billo, S.M. (1987) Petrology and kinetics of gypsum—anhydrite transitions. Journal of Petroleum Geology, 10, 73-85.

Bishop, J.L. and Murad E. (1996) Schwertmannite on Mars? Spectroscopic analyses of schwertmannite, its relationship to other ferric minerals, and its possible presence in the surface material on Mars. In M. D. Dyar, C. McCammon, and M. W. Schaefer, Eds., Mineral Spectroscopy: A tribute to Roger G. Burns, Special Publication Number 5, 337-358. The Geochemical Society. Houston, TX.

Bishop, J.L. and Murad E. (2005) The visible and infrared spectral properties of jarosite and alunite. American Mineralogist, 90, 1100-1107.

Bishop, J.L., Murad E., Lane M.D., and Mancinelli R.L. (2004) Multiple techniques for mineral identification on Mars: A study of hydrothermal rocks as potential analogues for astrobiology sites on Mars. Icarus, 169, 331-323.

Blaney, D.L. and McCord T.B. (1995) Indications of sulfate minerals in the Martian soil from Earth-based spectroscopy. Journal of Geophysical Research, 100, 14433-14441.

Bromehead, C.E.N. (1943) The forgotten uses of selenite. Mineralogical Magazine, 182, 325-333.

Brown, A.J. (2006) Spectral curve fitting for automatic hyperspectral data analysis. IEEE Transactions on Geoscience and Remote Sensing, 44, 1601-1608.

Brown, A.J. and Cudahy T.J. (2006) Hyperspectral imaging of sulfate evaporite deposits in Western Australia and on Mars. SPIE Electronic Imaging, San Jose, CA.

Brown, A.J., Sutter B., and Dunagan S. (2008) The MARTE imaging spectrometer experiment: Design and analysis. Astrobiology, 8, 1001-1011.

589 Bundy, W.M. (1956) Petrology of gypsum-anhydrite deposits in southwestern Indiana.
590 Journal of Sedimentary Petrology, 26, 240-252.
591 Clark, R.N., King T.V.V., Klejwa M., and Swayze G.A. (1990) High spectral resolution
592 reflectance spectroscopy of minerals. Journal of Geophysical Research, 95, 12653-
593 12680.
594 Clark, R.N., Swayze G.A., Wise R., Livo E., Hoefen T., Kokaly R., and Sutley S.J. (2007) USGS
595 digital spectral library splib06aDigital Data Series 231. p. U.S. Geological Survey
596 Cloutis, E.A., Hawthorne F.C., Mertzman S.A., Krenn K., Craig M.A., Marcino D., Methot M.,
597 Strong J., Mustard J.F., Blaney D.L., Bell J.F., III, and Vilas F. (2006) Detection and
598 discrimination of sulfate minerals using reflectance spectroscopy. Icarus, 184, 121-
599 157.
600 Conley, R.F. and Bundy W.M. (1958) Mechanism of gypsification. Geochimica et
601 Cosmochimica Acta, 15, 57-72.
602 Crowley, J.K. (1991) Visible and near-infrared (0.4–2.5 μm) reflectance spectra of Playa
603 evaporite minerals. Journal of Geophysical Research: Solid Earth, 96, 16231-16240.
604 Deer, W.A., Howie R.A., and Zussman J. (1992) An Introduction to the Rock-Forming
605 Minerals. 528 p. Longman, London.
606 Dyar, M.D., Gunter M.E., and Tasa D. (2008) Mineralogy and Optical Mineralogy. 708 p.
607 Mineralogical Society, Chantilly, VA.
608 Fishbaugh, K.E., Poulet F., Chevrier V., Langevin Y., and Bibring J.-P. (2007) On the origin of
609 gypsum in the Mars north polar region. Journal of Geophysical Research, 112,
610 E07002 1-17.

611 Grotzinger, J.P., Arvidson R.E., Bell III J.F., Calvin W.M., Clark B.C., Fike D.A., Golombek M.,
612 Greeley R., Haldemann A., Herkenhoff K.E., Jolliff B.L., Knoll A.H., Malin M.C.,
613 McLennan S.M., Parker T., Soderblom L.A., Sohl-Dickstein J.N., Squyres S.W., Tosca
614 N.J., and Watters W.A. (2005) Stratigraphy and sedimentology of a dry to wet eolian
615 depositional system, Burns formation, Meridiani Planum, Mars. Earth and Planetary
616 Science Letters, 240, 11-72.
617 Gunatilaka, A., Al-Temeemi A., Saleh A., and Nassar N. (1985) A new occurrence of bassanite
618 in recent evaporitic environments, Kuwait, Arabian Gulf. Journal of the University of
619 Kuwait (Science), 12, 157-166.
620 Hapke, B. (1981) Bidirectional reflectance spectroscopy, 1. Theory. Journal of Geophysical
621 Research, 86, 3039-3054.
622 Hapke, B. (1993) Combined theory of reflectance and emittance spectroscopy. In C. M.
623 Pieters and P. A. J. Englert, Eds., Remote Geochemical Analysis: Elemental and
624 Mineralogical Composition, 31-42. Cambridge University Press. Cambridge.
625 Hardie, L.A. (1967) The gypsum-anhydrite equilibrium at one atmosphere pressure.
626 American Mineralogist, 52, 171-200.
627 Hardie, L.A. and Eugster H.P. (1971) The depositional environment of marine evaporites: A
628 case for shallow, clastic accumulation. Sedimentology, 16, 187-220.
629 Harrison, T.N. (2012) Experimental VNIR reflectance spectroscopy of gypsum dehydration:
630 Investigating the gypsum to bassanite transition. American Mineralogist, 97, 598-
631 609.
632 Hawthorne, F.C., Krivovichev S.V., and Burns P.C. (2000) The crystal chemistry of sulfate
633 minerals. In C. N. Alpers, J. L. Jambor, and D. K. Nordstrom, Eds., Sulfate Minerals:

634 Crystallography, Geochemistry, and Environmental Significance, 1-112. Reviews in
635 Mineralogy and Geochemistry, Volume 40. Washington, D.C.
636 Haynes, S.J., Boland R., and Hughes-Pearl J. (1989) Depositional setting of gypsum deposits,
637 southwestern Ontario; the Domtar Mine. Economic Geology, 84, 857-870.
638 Holland, H.D. (2002) Volcanic gases, black smokers, and the great oxidation event.
639 Geochimica et Cosmochimica Acta, 66, 3811-3826.
640 Hunt, G.R. and Vincent R.K. (1968) The behavior of spectral features in the infrared
641 emission from particulate surfaces of various grain sizes. Journal of Geophysical
642 Research, 73, 6039-6046.
643 Hunt, G.R., Salisbury J.W., and Lenhoff C.J. (1971) Visible and near-infrared spectra of
644 minerals and rocks: IV. Sulphides and sulphates. Modern Geology, 3, 1-14.
645 Innorta, G., Rabbi E., and Tomadin L. (1980) The gypsum-anhydrite equilibrium by
646 solubility measurements. Geochimica et Cosmochimica Acta, 44, 1931-1936.
647 Kushnir, J. (1982) The partitioning of seawater cations during the transformation of
648 gypsum to anhydrite. Geochim. Cosmochim. Acta, 46, 433-446.
649 Lane, M.D. (1999) Midinfrared optical constants of calcite and their relationship to particle
650 size effects in thermal emission spectra of granular calcite. Journal of Geophysical
651 Research, 104, 14099-14108.
652 Lane, M.D. (2007) Mid-infrared emission spectroscopy of sulfate and sulfate-bearing
653 minerals. American Mineralogist, 92, 1-18.
654 Lane, M.D. and Christensen P.R. (1998) Thermal infrared emission spectroscopy of salt
655 minerals predicted for Mars. Icarus, 135, 528-536.

Langevin, Y., Poulet F., Bibring J.-P., and Gondet B. (2005) Sulfates in the north polar region of Mars detected by OMEGA/Mars Express. Science, 307, 1584-1586.

Leitner, C., Neubauer F., Marschallinger R., Genser J., and Bernroider M. (2013) Origin of deformed halite hopper crystals, pseudomorphic anhydrite cubes and polyhalite in Alpine evaporites (Austria, Germany). International Journal of Earth Sciences, 102, 813-829.

Logan, L.M., Hunt G.R., and Salisbury J.W. (1975) The use of mid-infrared spectroscopy in remote sensing of space targets. In C. Karr, Eds., Infrared and Raman Spectroscopy of Lunar and Terrestrial Minerals, 117-142. Academic Press. New York.

Ludwig, C.F. (1804) Handbuch der Mineralogie nach A. G. Werner p. Siegfried Lebrecht Crusius, Leipzig.

McMillan, P.F. and Hofmeister A.M. (1988) Infrared and Raman spectroscopy. In F. C. Hawthorne, Eds., Spectroscopic Methods in Mineralogy and Geology, 99-159. Mineralogical Society of America. Washington DC.

Meijer, J.A.M. (1984) Inhibition of calcium sulfate depositions by a fluidized bed. Desalination, 52, 25-42.

Miller, F.A. and Wilkins C.H. (1952) Infrared spectra and characteristic frequencies of inorganic ions. Analytical Chemistry, 24, 1253-1294.

Miller, F.A., Carlson G.L., Bentley F.F., and Jones W.H. (1960) Infrared spectra of inorganic ions in the cesium bromide region (700-300 cm-1). Spectrochim. Acta, 16, 135-235.

Moenke, H. (1962) Mineralspektren I: Die Ultrarotabsorption der häufigsten und wirtschaftlich wichtigsten Halogenid-, Oxyd-, Hydroxyd-, Carbonat-, Nitrat-, Borat-,

678 Sulfat-, Chromat-, Wolframat-, Molybdat-, Phosphat-, Arsenat-, Vanadat- und
679 Silikatmineralien im Spektralbereich 400-4000 cm-1 p. Akademie-Verlag, Berlin.
680 Murray, R.C. (1964) Origin and diagenesis of gypsum and anhydrite. Journal of Sedimentary
681 Petrology, 34, 512-523.
682 Mustard, J.F. and Hays J.E. (1997) Effects of hyperfine particles on reflectance spectra from
683 0.3 to 25 μm. Icarus, 125, 145-163.
684 Ostroff, A.G. (1964) Conversion of gypsum to anhydrite in aqueous salt solutions.
685 Geochimica et Cosmochimica Acta, 28, 1363-1372.
686 Posnjak, E. (1940) Deposition of calcium sulfate from sea water. American Journal of
687 Science, 238, 559-568.
688 Prasad, P.S.R., Pradhan A., and Gowd T.N. (2001) In situ micro-Raman investigation of
689 dehydration mechanism in natural gypsum. CURRENT SCIENCE, 80, 1203-1207.
690 Prasad, P.S.R., Chaitanya V.K., Prasad K.S., and Rao D.N. (2005) Direct formation of the γ-
691 $CaSO_4$ phase in degydration process of gypsum: In situ FTIR srudy. American
692 Mineralogist, 90, 672-678.
693 Prothero, D.R. and Schwab F. (2004) Sedimentary Geology. An Introduction to Sedimentary
694 Rocks and Stratigraphy p. W. H. Freeman and Co., New York.
695 Robertson, E.C., Robie R.A., and Books K.G. (1958) Physical properties of salt, anhydrite,
696 and gypsum. p. US Geologic Survey, Denver.
697 Ross, S.D. (1974) Sulphates and other oxy-anions of Group VI. In V. C. Farmer, Eds., The
698 Infrared Spectra of Minerals, 423-444. The Mineralogical Society. London.

699 Ruff, S.W., Christensen P.R., Barbera P.W., and Anderson D.L. (1997) Quantitative thermal
700 emission spectroscopy of minerals: A technique for measurement and calibration.
701 Journal of Geophysical Research, 102, 14,899 - 14,913.
702 Salisbury, J.W. (1993) Mid-infrared spectroscopy: Laboratory data. In C. M. Pieters and P. A.
703 J. Englert, Eds., Remote Geochemical Analysis: Elemental and Mineralogical
704 Composition, 79-98. Cambridge University Press. Cambridge.
705 Salisbury, J.W. and Wald A. (1992) The role of volume scattering in reducing spectral
706 contrast of reststrahlen bands in spectra of powdered minerals. Icarus, 96, 121-128.
707 Salisbury, J.W., Walter L.S., Vergo N., and D'Aria D.M. (1991) Infrared (2.1-25 μm) Spectra of
708 Minerals. 267 p. Johns Hopkins University Press, Baltimore.
709 Sievert, T., Wolter A., and Singh N.B. (2005) Hydration of anhydrite of gypsum (CaSO4.II) in
710 a ball mill. Cement and Concrete Research, 35, 623-630.
711 Singh, M. and Garg M. (1995) Activation of gypsum anhydrite-slag mixtures. Cement and
712 Concrete Research, 25, 332-338.
713 Singh, N.B. and Middendorf B. (2007) Calcium sulphate hemihydrate hydration leading to
714 gypsum crystallization. Progress in Crystal Growth and Characterization of
715 Materials, 53, 57-77.
716 Squyres, S.W. (2012) Initial Opportunity rover results at Endeavour Crater, Mars Lunar
717 Planet Sci. Conf., The woodlands, TX, abs. # 1892.
718 Szumila, I., Bishop J.L., Fenton L.K., and Brown A.J. (2013) Composition and morphology of
719 gypsum dunes in Olympia Undae on Mars. Lunar Planet. Sci. Conf., The Woodlands,
720 TX, Abstract #2123.

721 Szynkiewicz, A., Ewing R.C., Moore C.H., Glamoclija M., Bustos D., and Pratt L.M. (2010)
722 Origin of terrestrial gypsum dunes—Implications for Martian gypsum-rich dunes of
723 Olympia Undae. Geomorphology, 121, 69-83.
724 Weitz, C.M., Bishop J.L., and Grant J.A. (2013a) Gypsum, opal, and fluvial channels within a
725 trough of Noctis Labyrinthus, Mars: Implications for aqueous activity during the
726 Late Hesperian to Early Amazonian. Planet. Space Sci, 87, 130-145.
727 Weitz, C.M., Noe Dobrea E.Z., and Wray J.J. (2013b) Mixtures of clays and sulfates within
728 deposits in western Melas Chasma. Icarus, submitted.
729 Wenrich, M.L. and Christensen P.R. (1996) Optical constants of minerals derived from
730 emission spectrocopy: Application to quartz. Journal of Geophysical Research, 101,
731 15921-15931.
732 Worku, T. and Parker A. (1992) Occurrence of bassanite in Lower Lias rocks of the Lyme
733 Regis area, England. Mineralogical Magazine, 56, 258-259.
734 Wray, J.J., Squyres S.W., Roach L.H., Bishop J.L., Mustard J.F., and Noe Dobrea E.Z. (2010)
735 Identification of the Ca-sulfate bassanite in Mawrth Vallis, Mars. Icarus, 209, 416-
736 421.
737 Zambonini, F. (1910) Mineralogia Vesuviana. Mem. Acc. Sc. Napoli, 14, 327-328.
738 Zhang, Q., Kasai E., and Saito F. (1996) Mechanochemical changes in gypsum when dry
739 ground with hydrated minerals. Powder Technology, 87, 67-71.
740

741 Table 1 Summary of Spectral Features for Ca-sulfates
742

Mineral	Location	Grain size (μm)	Sample ID #	Reference
gypsum	Niedersachswerfen, Nordhausen, Harz, Germany	<45, 45-90, 90-125, 125-250, >250	JB1464	this study, from Gunnar Farber Mineralien
Gypsum*/ bassanite	Mule Canyon, CA	<63	ML-S6, JB556	Lane and Christensen 1998
gypsum	Mule Canyon, CA	63-90	ML-S6, JB557	Lane and Christensen 1998
gypsum	Eddy County, NM	rock surface	ML-S8	Lane and Christensen 1998
gypsum	Italy	<75, 75-250, rock surface, KBr pellet	26B	Hunt et al. 1971; Salisbury et al. 1991
gypsum	Vermont	<75, 75-250, rock surface, KBr pellet	333B	Hunt et al. 1971; Salisbury et al. 1991
bassanite	synthetic	50-1000	GDS145	Crowley et al. 1991; Clark et al. 2007
bassanite		rock surface	ML-S11	Lane and Christensen 1998
anhydrite	Djebel Melah d'El Outaya, Massif de l'Aures, Biskra, Hautes Plateau, Algeria	rock surface	JB641, DD102	this study, from mineral dealer
anhydrite	Carson City, NV	rock surface	ML-S16	Lane and Christensen 1998
anhydrite	France	<75, 75-250, rock surface, KBr pellet	NMNH46393	Salisbury et al. 1991
anhydrite	New Mexico	<250 (ave ~150)	GDS42	Clark et al. 2007

743
744 Notes: *sample ML-S6 was gypsum at the time emission spectra were obtained, but had
745 partially altered to bassanite by the time the reflectance spectra were acquired.
746
747

Table 2 Summary of Spectral Features for Ca-sulfates

	Anhydrite $Ca(SO_4)$	Bassanite $Ca(SO_4) \bullet 0.5H_2O$	Gypsum $Ca(SO_4) \bullet 2H_2O$
NIR bands in μm (and cm^{-1})			
H_2O		1.344 (7440)	
combinations		1.428, 1.476, 1.54	1.446, 1.490, 1.538
and overtones		(7003, 6775, 6494)	(6916, 6711, 6502)
		1.78 (5618)	1.750 (5714)
		1.93 (5181)	1.942 (5149)
		2.10 (4762)	
		2.164 (4621)	2.178 (4591)
		2.219 (4507)	2.217 (4511)
		2.262, 2.268	2.268 (4409)
		(4421, 4409)	
		2.484 (4026)	2.486 (4023)
H_2O stretch	~2.9	2.75-3.1	2.75-3.1
	(~3450)	(~3640-3230)	(~3640-3230)
SO_4	3.924	3.871, 3.968, 4.004	3.871, 3.975
combinations	(2548)	(2583, 2520, 2498)	(2583, 2516)
and	4.203, 4.286, 4.348		
overtones	(2379, 2333, 2300)		
	4.469 (2238)	4.506 (2219)	4.487 (2229)
	4.668, 4.691 (2142, 2132)	4.688 (2142)	4.689 (2133)
	4.925 (2030)	4.966 (2014)	4.972 (2011)
mid-IR peaks in cm^{-1} (and μm)			
↓ H_2O bend	1693 (5.91)	1684 (5.94)	1681 (5.95)
↓ H_2O bend	1623 (6.16)	1628 (6.14)	1630 (6.13)
↓ H_2O bend	1545* (6.47)	~1500* (6.67)	~1530* (6.54)
↑ SO_4 ν_3	1197, 1156 (8.35, 8.65)	1169, 1157 (8.55, 8.64)	1195, 1154 (8.37, 8.67)
↓ SO_4 ν_1	1015* (9.85)	1012* (9.88)	1005* (9.95)
↑ SO_4 ν_4	687 (14.6)	663 (15.1)	673 (14.9)
↑ SO_4 ν_4	619, 597 (16.2, 16.8)	598 (16.7)	604 (16.6)
↓ SO_4 ν_2	510* (19.6)	~490 (20.4)	~470 (21.3)
↑	266 (37.6)	240, 225 (41.7, 44.4)	

Notes: *band is present for fine-grained samples; arrows indicate if the feature is present as an absorption (down) or a peak (up).

789 **Figure Captions**

790

791 Figure 1. Comparison of the structures of anhydrite, bassanite, and gypsum, which are all
792 based on the large coordination polyhedron of the Ca^{2+} cation. All three structures consist
793 of Ca polyhedra sharing edges with SO_4 tetrahedra to form chains. The structures differ by
794 how the chains are connected, and by how many corners of the Ca polyhedra are shared
795 with H_2O.

796

797 Figure 2 VNIR reflectance spectra from 0.35 to 5.0 μm of selected Ca-sulfates measured in
798 a dry environment: fine-grained anhydrite from Algeria, fine-grained anhydrite from
799 France, bassanite synthesized from gypsum, altered (dehydrated) gypsum and gypsum.
800 The grey lines mark bands and facilitate observation of differences in the spectral features
801 of gypsum, bassanite and anhydrite.

802

803 Figure 3 Continuum-removed spectra of hydrated Ca-sulfates across the 1.28-1.6 μm
804 region.

805

806 Figure 4 Continuum-removed spectra of several Ca-sulfates across the 2.05-2.35 μm
807 region.

808

809 Figure 5 Continuum-removed spectra of several Ca-sulfates across the 3.8-5.0 μm region.

810

Figure 6 Mid-IR reflectance spectra of several Ca-sulfates: fine-grained anhydrite from Algeria, fine-grained anhydrite from France (Salisbury et al 1991), bassanite synthesized from gypsum, dehydrated gypsum and gypsum (Lane 2007).

Figure 7 Mid-IR spectra of several Ca-sulfates including emission spectra from Lane (2007): a) anhydrite, b) fine-grained bassanite, and c) gypsum, and hemispherical reflectance spectra from Salisbury et al. (1991): d) an anhydrite sample from France, e) a gypsum cleavage face from Vermont and f) a gypsum sawn surface from Italy.

Figure 8 Mid-IR transmittance spectra of anhydrite and gypsum Salisbury et al. (1991).

Figure 9 Mid-IR reflectance and transmittance spectra of a) anhydrite from France and b) gypsum from Italy (data from Salisbury et al. 1991). The reflectance spectra include a fracture surface for the anhydrite and a sawn surface for the gypsum.

Figure 10 Mid-IR reflectance spectra from 100-1800 cm^{-1} of multiple grain size fractions of gypsum and emission spectra of the >250 μm size fraction.

Figure 11 VNIR reflectance spectra from 0.4-5 μm of multiple grain size fractions of gypsum.

833 Figure 12 VNIR reflectance spectra from 0.35-2.55 μm of three grain size fractions of
834 gypsum measured under ambient (solid line) and dehydrated (dashed line) moisture
835 conditions.
836

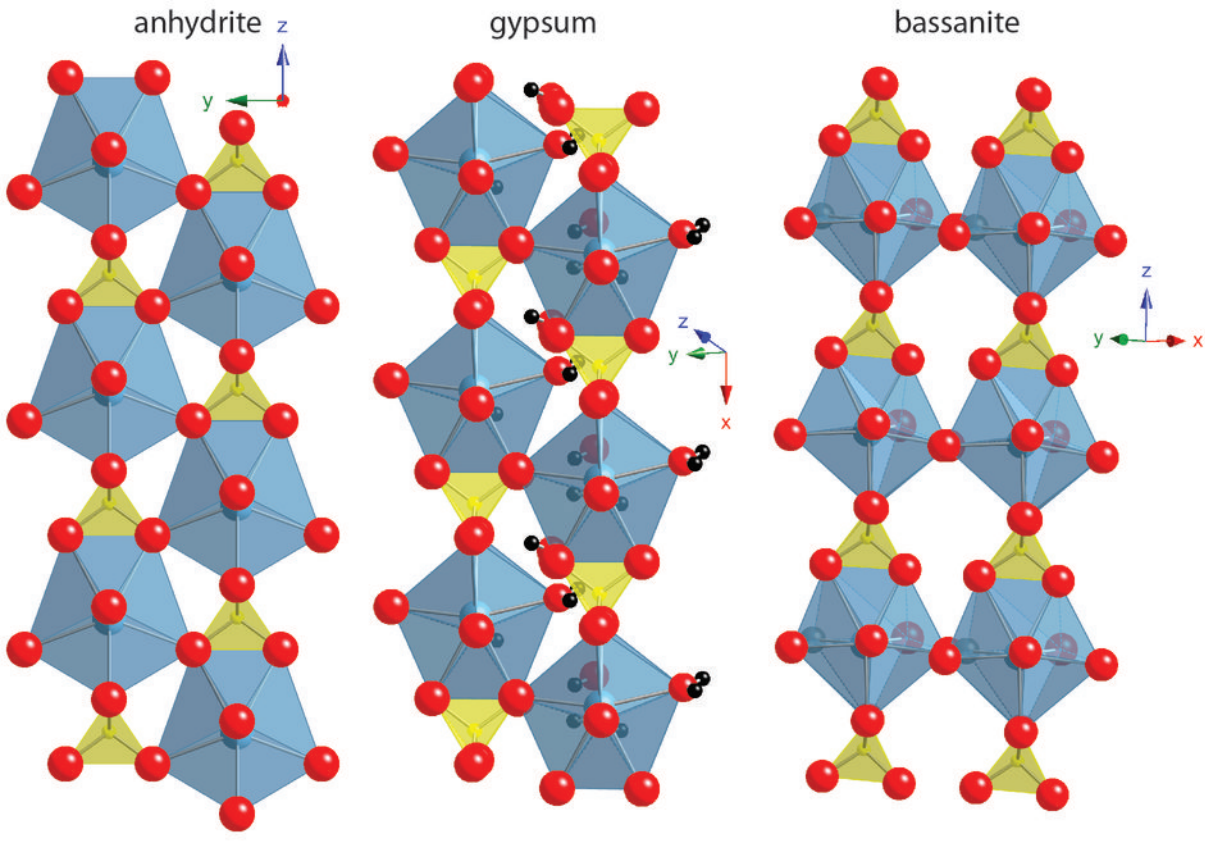
anhydrite
z
y
gypsum
z
y
x
bassanite
z
y
x

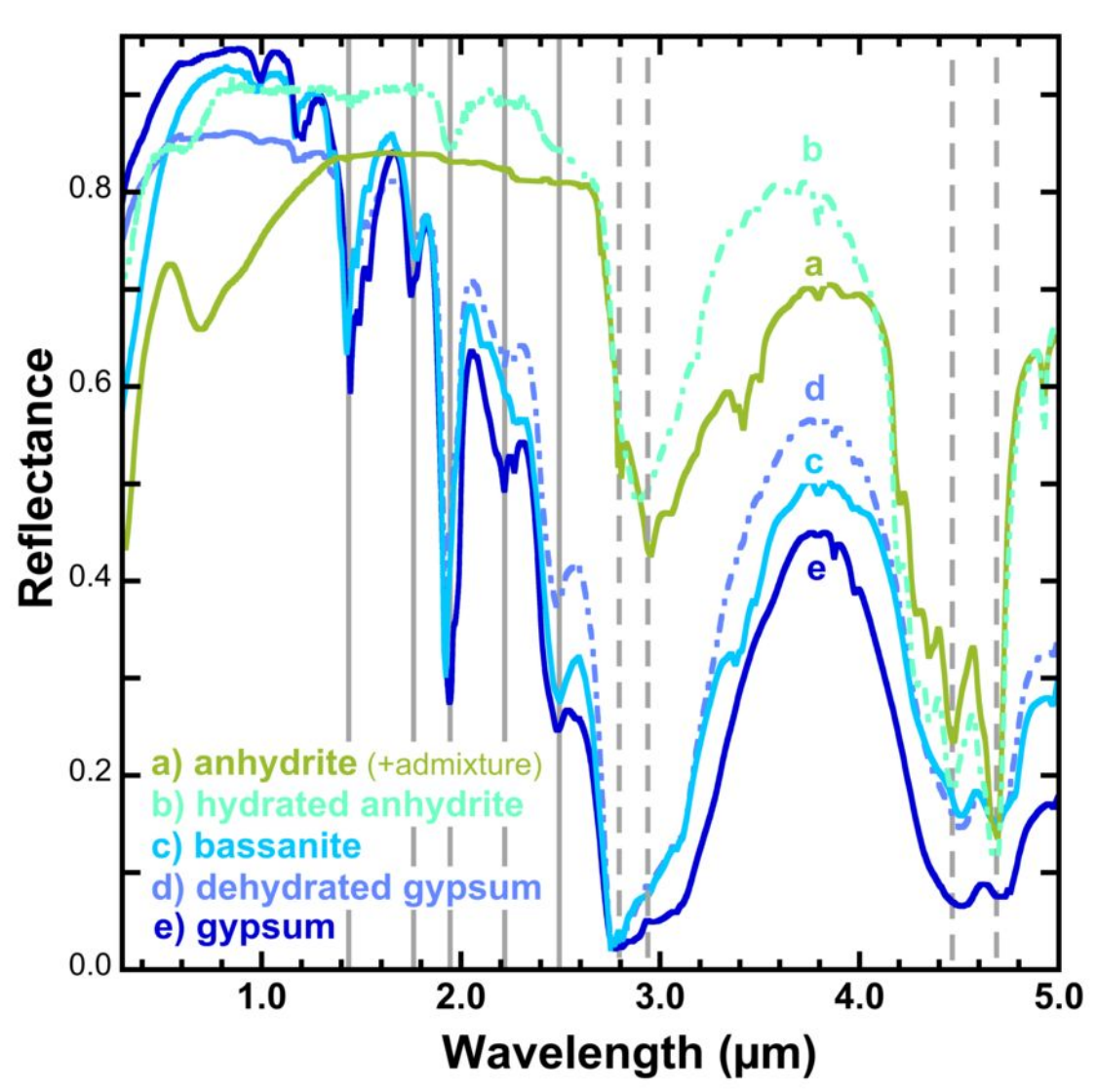
Reflectance
0.0
0.2
0.4
0.6
0.8
1.0
2.0
3.0
4.0
5.0
Wavelength (μm)
a) anhydrite (+admixture)
b) hydrated anhydrite
c) bassanite
d) dehydrated gypsum
e) gypsum
a
b
c
d
e

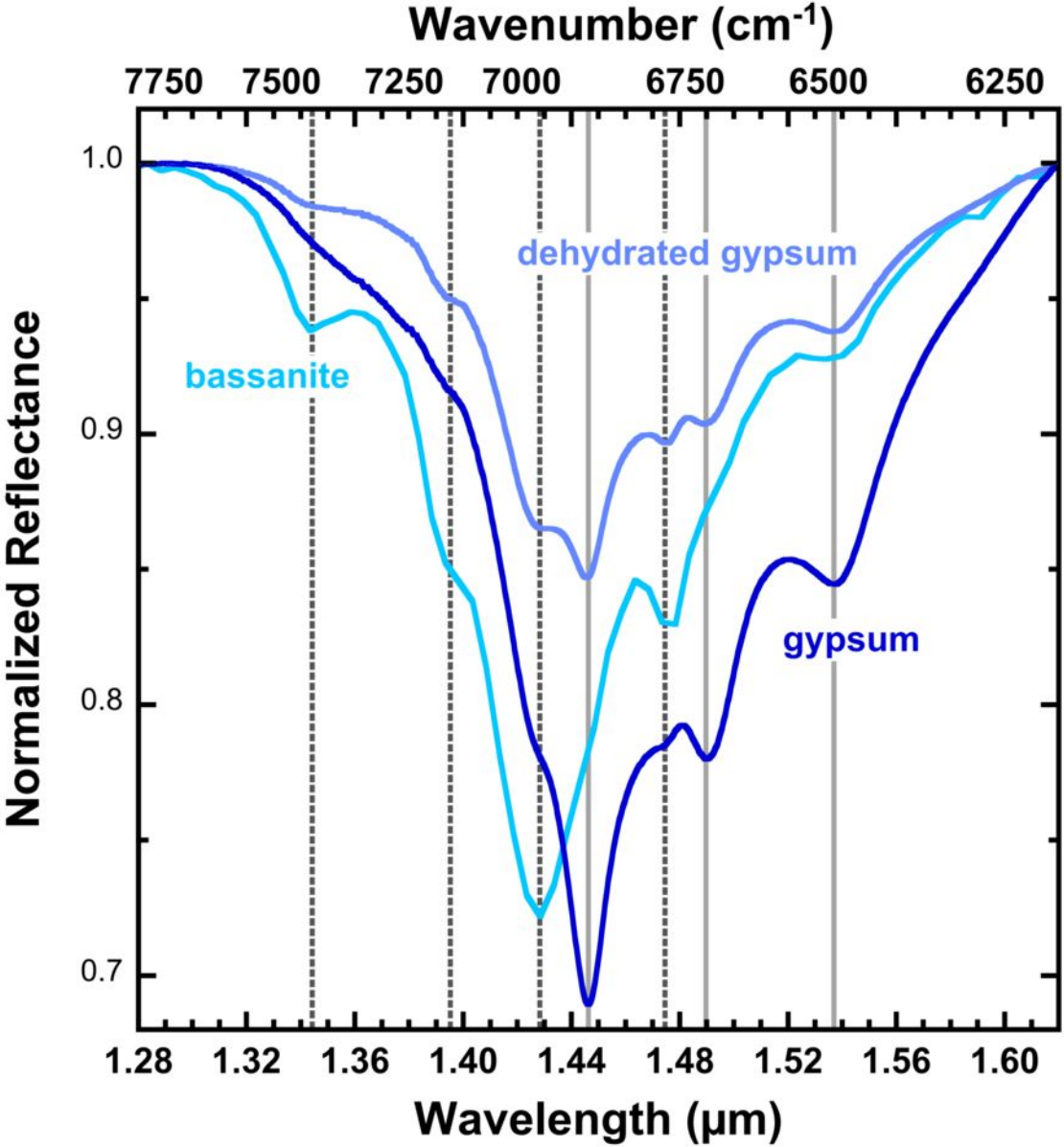
Wavenumber (cm-1)
7750
7500
7250
7000
6750
6500
6250
1.0
0.9
0.8
0.7
Normalized Reflectance
dehydrated gypsum
bassanite
gypsum
1.28
1.32
1.36
1.40
1.44
1.48
1.52
1.56
1.60
Wavelength (μm)

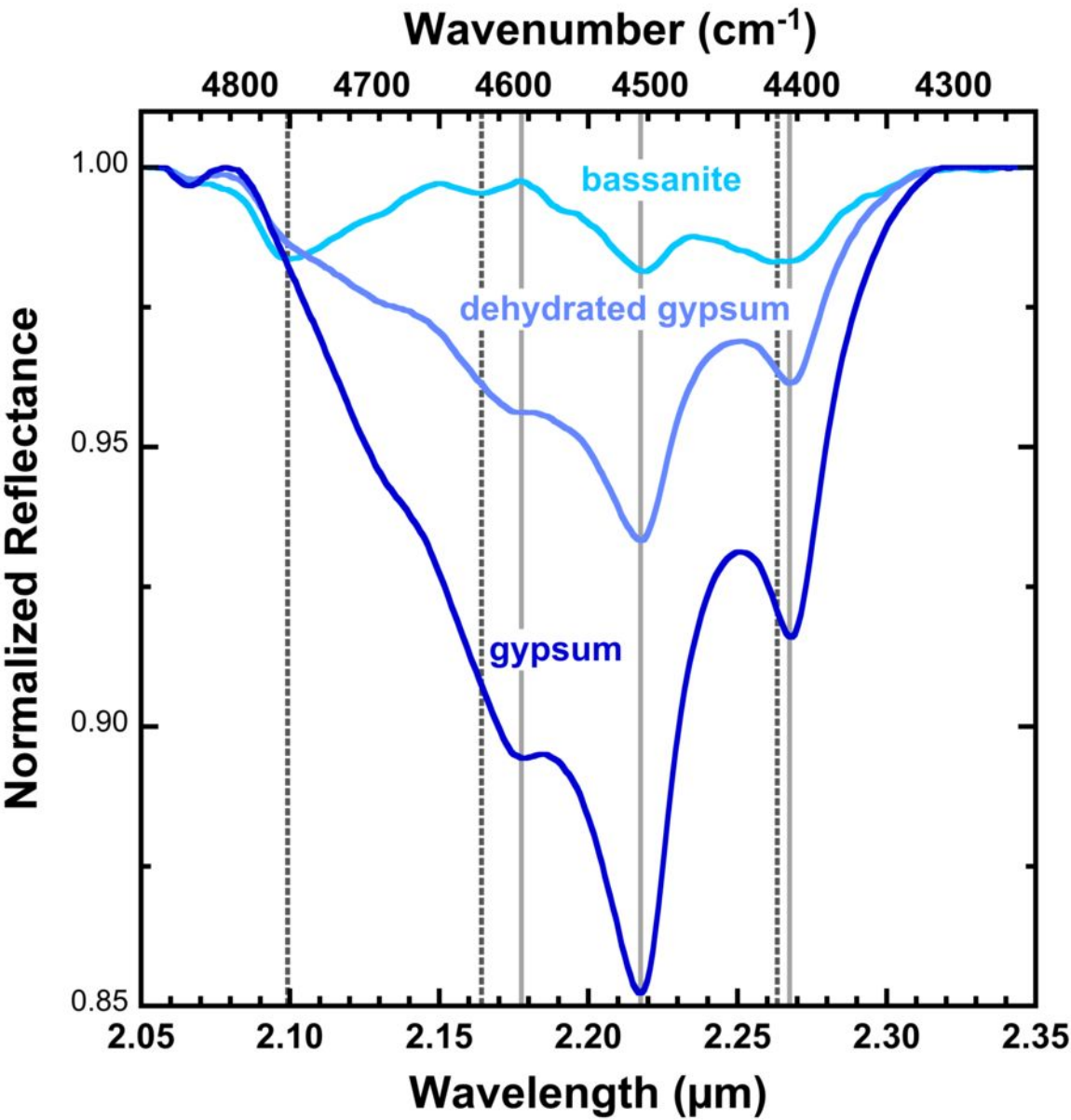
Wavenumber (cm-1)
4800
4700
4600
4500
4400
4300
1.00
0.95
0.90
0.85
Normalized Reflectance
bassanite
dehydrated gypsum
gypsum
2.05
2.10
2.15
2.20
2.25
2.30
2.35
Wavelength (μm)

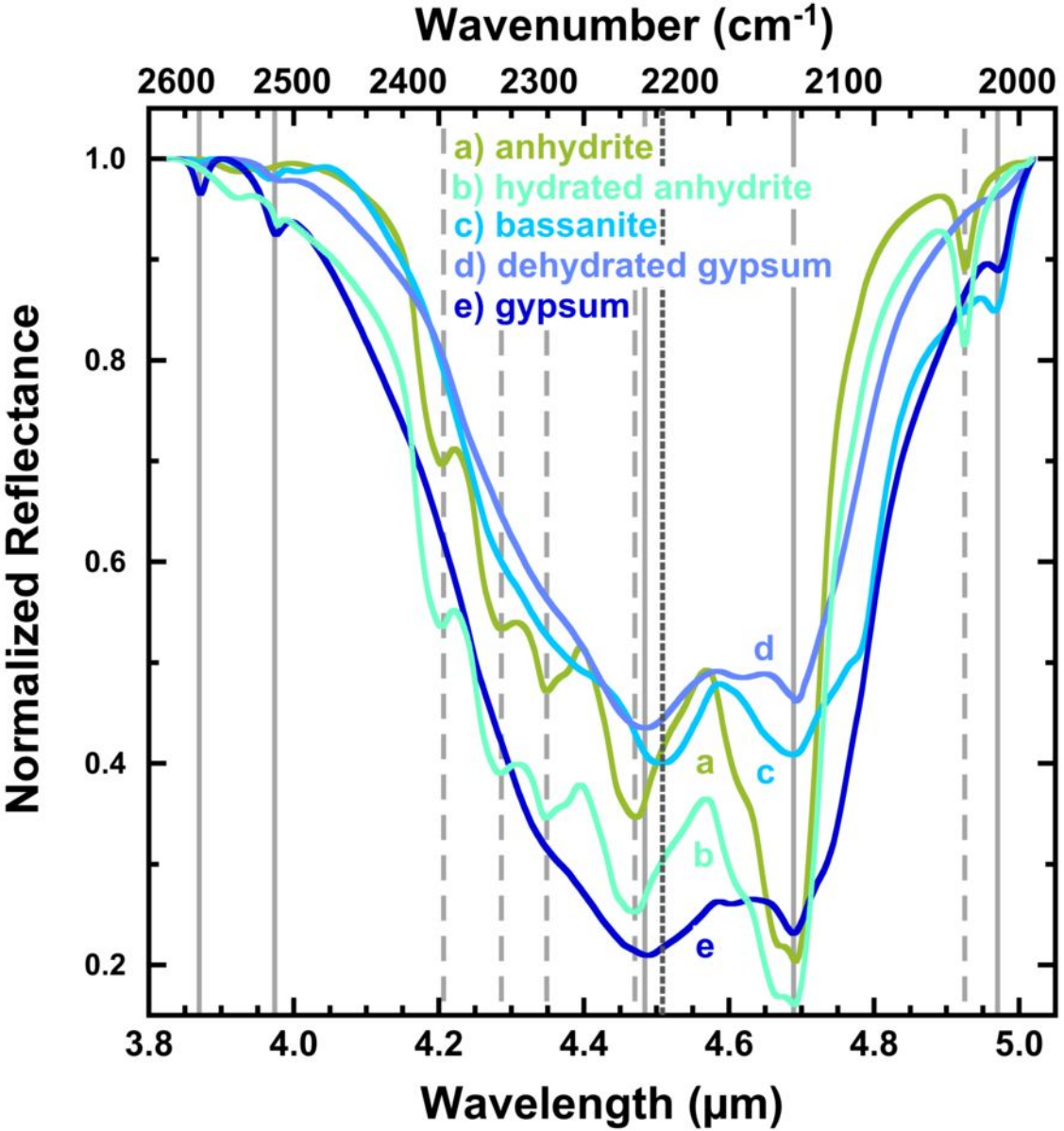
Wavenumber (cm-1)
2600
2500
2400
2300
2200
2100
2000
a) anhydrite
b) hydrated anhydrite
c) bassanite
d) dehydrated gypsum
e) gypsum
Normalized Reflectance
1.0
0.8
0.6
0.4
0.2
d
a
c
b
e
3.8
4.0
4.2
4.4
4.6
4.8
5.0
Wavelength (μm)

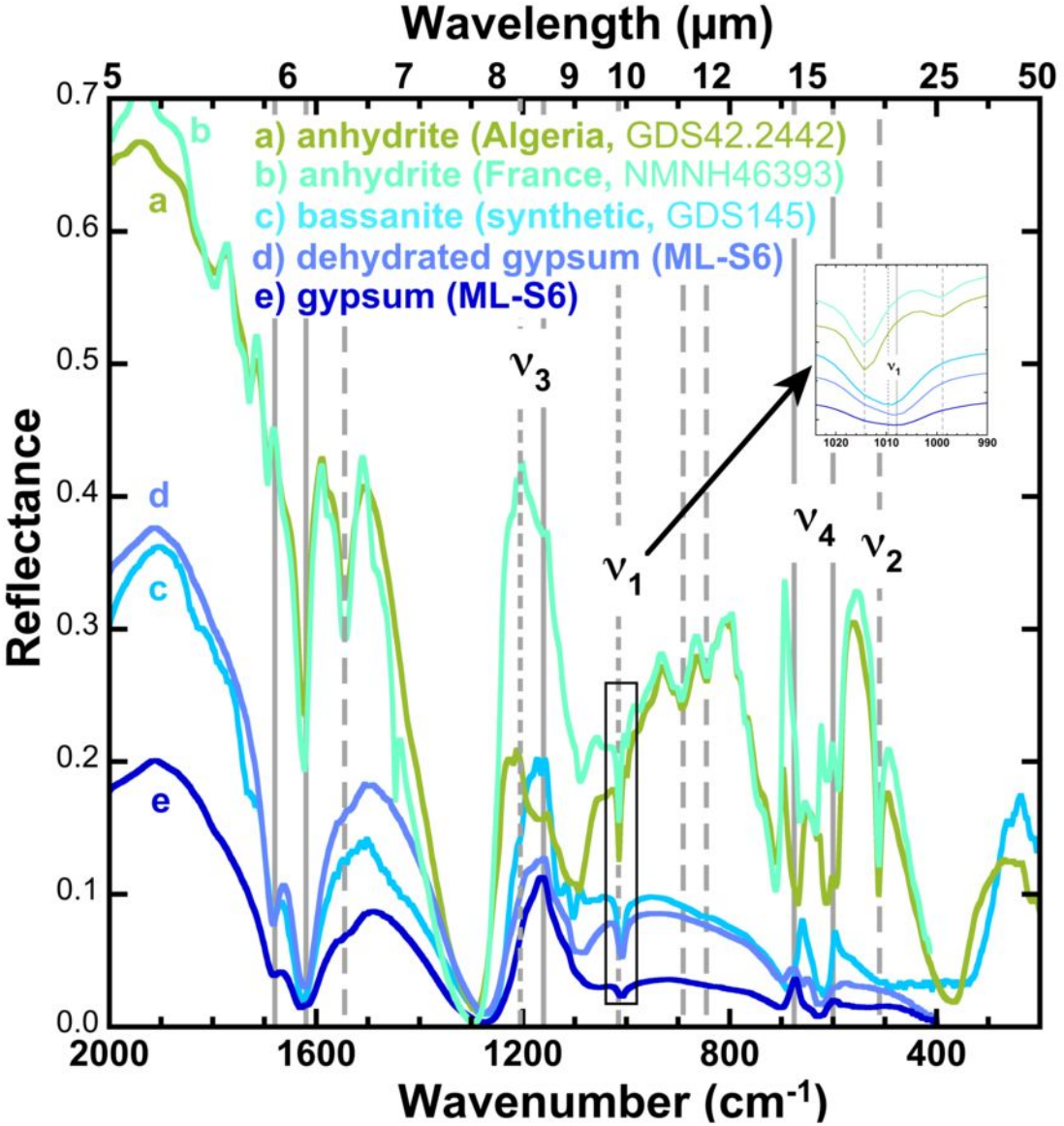
Wavelength (μm)
5
6
7
8
9
10
12
15
25
50
a) anhydrite (Algeria, GDS42.2442)
b) anhydrite (France, NMNH46393)
c) bassanite (synthetic, GDS145)
d) dehydrated gypsum (ML-S6)
e) gypsum (ML-S6)
a
b
c
d
e
ν3
ν1
ν4
ν2
1020
1010
1000
990
Reflectance
0.0
0.1
0.2
0.3
0.4
0.5
0.6
0.7
2000
1600
1200
800
400
Wavenumber (cm-1)

Wavelength (μm)

6 7 8 9 10 12 15 20 30 50

Emissivity

1.0 0.9 0.8 0.7

Reflectance

0.8 0.6 0.4 0.2 0.0

a) anhydrite
b) bassanite
c) gypsum
d) anhydrite surface
e) gypsum cleavage face
f) gypsum surface

a b c d e f

1800 1600 1400 1200 1000 800 600 400 200

Wavenumber (cm^{-1})

Wavelength (μm)

3 4 5 6 7 8 10 14 20

b

a

100 80 60 40 20 0

Transmittance

a) anhydrite France

b) gypsum Italy

ν_1

H_2O stretch

H_2O bend

ν_4

ν_3

4000 3500 3000 2500 2000 1500 1000 500

Wavenumber (cm^{-1})

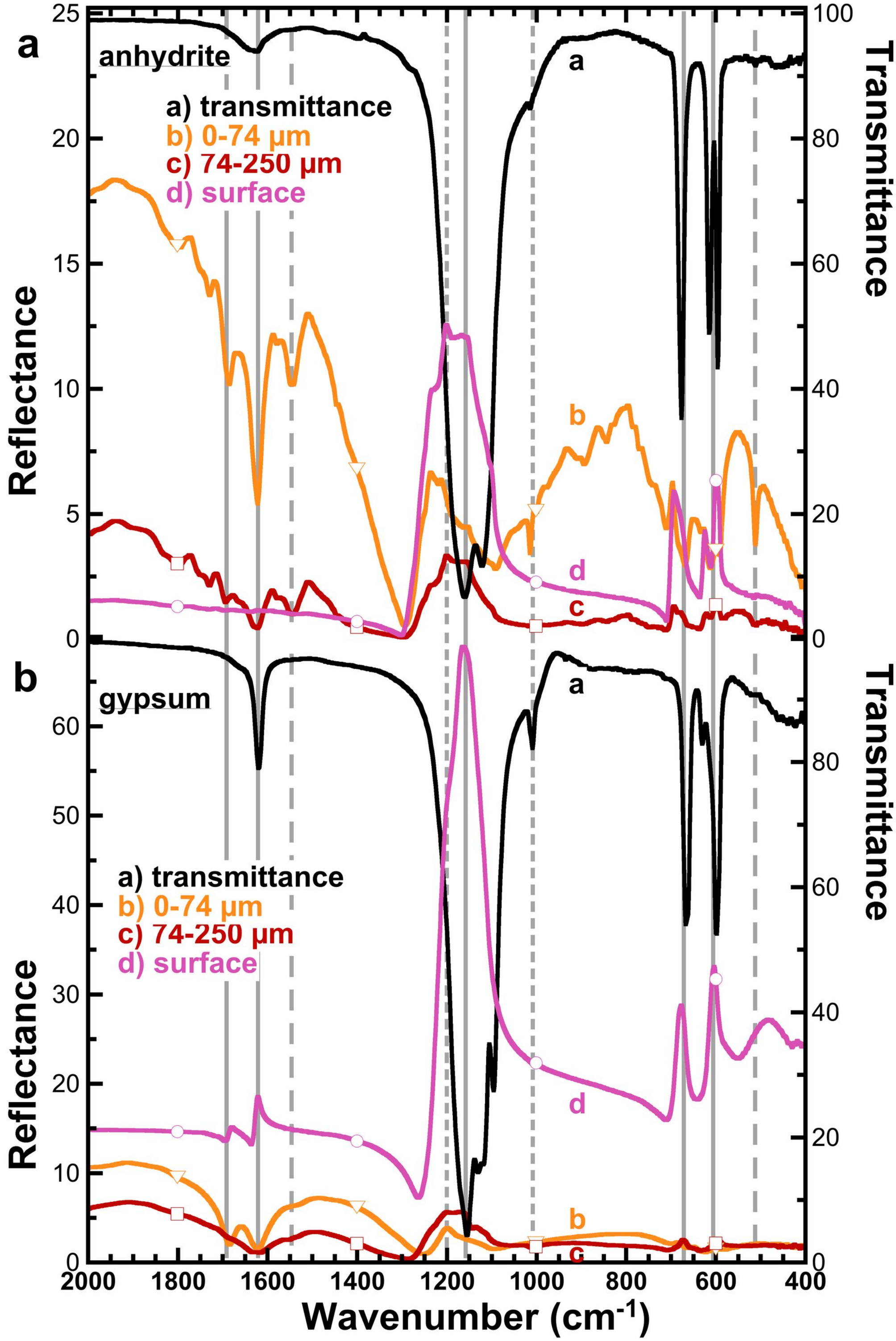
a
anhydrite
a) transmittance
b) 0-74 µm
c) 74-250 µm
d) surface
Reflectance
Transmittance
b
gypsum
Wavenumber (cm-1)
2000
1800
1600
1400
1200
1000
800
600
400

Wavelength (μm)

6 7 8 9 10 12 15 20 30 50

Reflectance

0.4 0.3 0.2 0.1 0.0

Emissivity

1.0 0.9 0.8

a) <45 μm
b) 45-90 μm
c) 90-125 μm
d) 125-250 μm
e) >250 μm

a b c d e

1800 1600 1400 1200 1000 800 600 400 200

Wavenumber (cm^{-1})

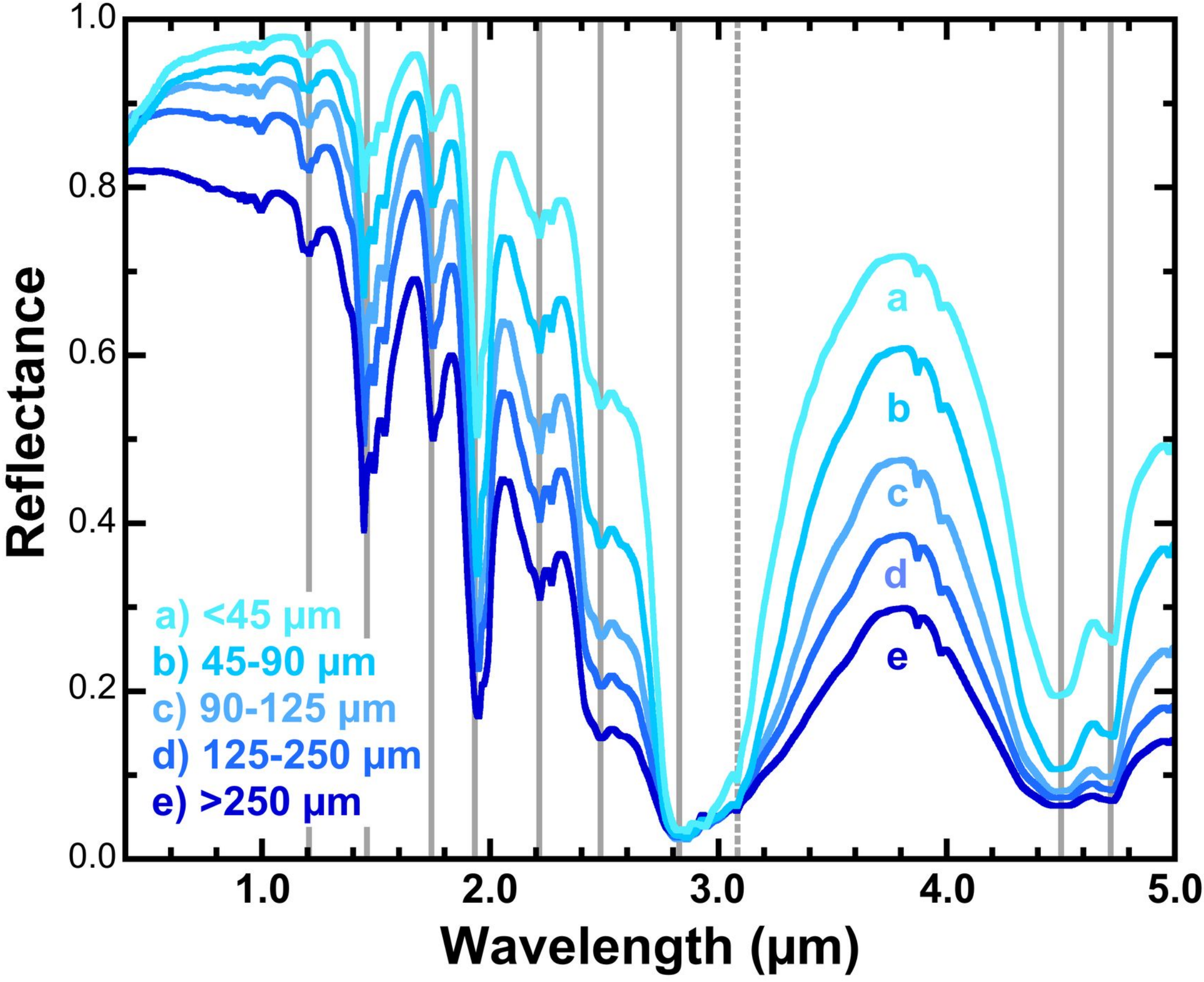
Reflectance
Wavelength (μm)
1.0
0.8
0.6
0.4
0.2
0.0
1.0
2.0
3.0
4.0
5.0
a
b
c
d
e
a) <45 μm
b) 45-90 μm
c) 90-125 μm
d) 125-250 μm
e) >250 μm

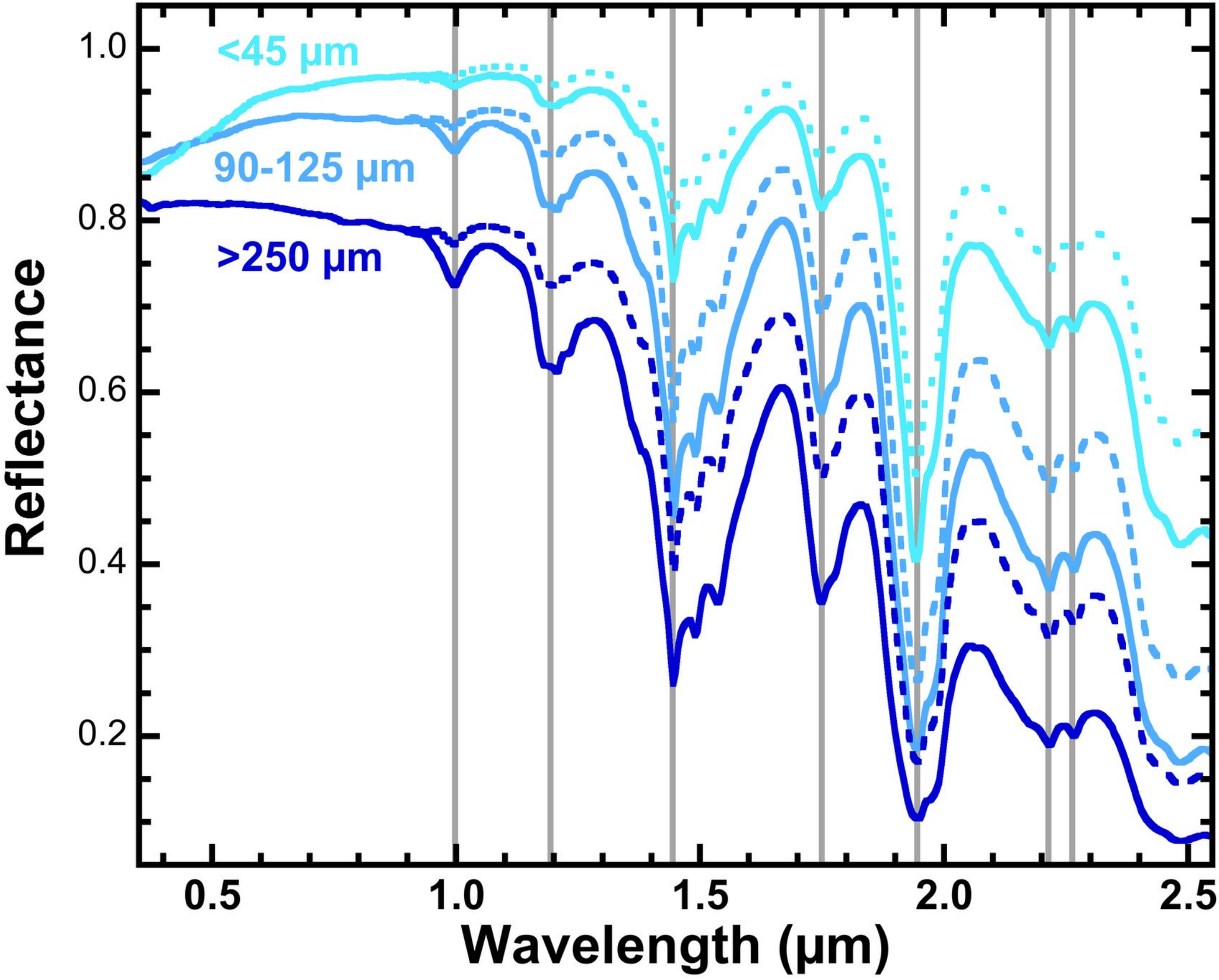
<45 µm
90-125 µm
>250 µm
Reflectance
1.0
0.8
0.6
0.4
0.2
0.5
1.0
1.5
2.0
2.5
Wavelength (µm)